ELSEVIER

Earth and Planetary Science Letters 201 (2002) 1–12

EPSL

www.elsevier.com/locate/epsl

Shock temperature in calcite ($CaCO_3$) at 95–160 GPa

Satish C. Gupta [1], Stanley G. Love [2], Thomas J. Ahrens *

Lindhurst Laboratory of Experimental Geophysics, Seismological Laboratory, California Institute of Technology, Pasadena, CA 91125, USA

Received 12 February 2002; accepted 13 April 2002

Abstract

The temperatures induced in crystalline calcite ($CaCO_3$) upon planar shock compression (95–160 GPa) are reported from two-stage light gas gun experiments. Temperatures of 3300–5400 K are obtained by fitting six-channel optical pyrometer radiances in the 450–900 nm range to the Planck gray-body radiation law. Thermodynamic calculations demonstrate that these temperatures are some 400–1350 K lower than expected for vibronic excitations of the lattice with a $3R$/mole-atom specific heat (R is gas constant). The temperature deficit along the Hugoniot is larger than that expected from only melting. In addition to melting, it appears likely that shock-induced decomposition of calcite occurs behind the shock front. We modeled disproportionation of calcite into CaO (solid) plus CO_2 (gas). For temperature calculations, specific heat at constant volume for 1 mole of CO_2 is taken to be $6.7R$ as compared to $9R$ in the solid state; whereas a mole of calcite and a mole of CaO have their solid state values $15R$ and $6R$, respectively. Calculations suggest that the calcite decomposes to CaO and CO_2 at $\sim 110 \pm 10$ GPa along the Hugoniot. Recent reanalysis of earlier VISAR measurements of particle velocity profiles [1] indicates that calcite shocked to 18 GPa undergoes disproportionation at much lower pressures upon isentropic expansion.

Keywords: calcite; shock metamorphism; volatilization; melting

1. Introduction

Research on the shock-induced devolatilization behavior of calcite has been motivated by the need to understand the role CO_2 gas has played in the formation and evolution of the atmosphere of Earth, and especially the planets, Mars [2] and Venus [3]. The Earth, and, probably, Mars and Venus have long been thought to contain substantial amounts of carbonates in their crusts. If abundant carbonates are, or were once, present in the Martian crust, definition of the shock pressure required to volatilize substantial quantities of CO_2 can be used to define the cratering rate and time interval over which Mars, operating a CO_2 greenhouse, became warm enough to support a liquid H_2O surface reservoir that was available to host life on the planet. Many observers of

* Corresponding author. Tel.: +1-626-395-6905; Fax: +1-626-564-0715.
E-mail address: tja@caltech.edu (T.J. Ahrens).

[1] Present address: High Pressure Physics Division, Bhabha Atomic Research Centre, Mumbai 400 085, India.
[2] Present address: Mail code CB, NASA Johnson Space Center, Houston, TX 77058, USA.

0012-821X/02/$ – see front matter
PII: S0012-821X(02)00685-4

Mars have concluded that the moderately mature and wide range of erosional structures, ubiquitous on the older hemisphere of Mars, require water for erosion. Understanding the role of shock devolatilization is also important to evaluate the mechanisms of impact induced extinction of marine and terrestrial biota at, for example, the K/T boundary. It is now widely accepted that this extinction is related to the impact on Earth of a large bolide [4]. Many researchers who have been concerned about extinction mechanisms now accept that sulfuric acid stratospheric aerosol induced reduction in solar insolation resulting in global cooling [5] (first proposed by Brett [6]) led to mass killing. The recent discovery of the Chicxulub crater as the impact site and related studies suggesting the presence of about 70% carbonates (limestone and dolomite) in the upper 3 km thick layer at this site [7] have raised the possibility of extinction mechanisms acting over a longer duration (10^0–10^4 yr) [8] arising from a global greenhouse heating event at the K/T boundary. Such longer duration heating is not precluded by our present very general knowledge of the climate of Earth. This has provided further motivation for research efforts on defining the shock-induced behavior of calcite.

Previously several theoretical and experimental studies have focused on the shock devolatilization behavior of calcite. Kieffer and Simonds [9] obtained a theoretical estimate of post-shock energy content. They assumed release isentropes could be approximated by the Hugoniot itself and determined that isentropic release from a shock pressure of 45 GPa resulted in incipient devolatilization. Vizgirda and Ahrens [10] actually determined release isentropes for aragonite and calculated post-shock energy content as a function of pressure for calcite and aragonite and determined that isentropic release of calcite from a Hugoniot pressure of 33 GPa resulted in incipient vaporization. Also, Boslough et al. [11] used a gas phase recovery technique during shock compression and decompression and found that a small fraction, 0.03–0.3 mole%, of calcite was devolatilized upon exposure to $\sim$17–18 GPa. Lange and Ahrens [12], on the other hand, used a solid recovery method to measure shock-induced CO_2 loss for single-crystal calcite up to 42 GPa peak pressure, and found in agreement with Boslough et al. [11], that CO_2 loss occurs around pressures as low as 10 GPa. Extrapolating their data, they determined that complete loss of CO_2 would occur around 70 GPa. The fact that devolatilization of calcite occurred upon exposure to shock pressures lower than the theoretical values of Kieffer and Simonds [9] and Vizgirda and Ahrens [10] has been attributed to heterogeneous heating (shear banding) of calcite [13].

To further examine the vaporization criterion of calcite, recently Yang [14] carried out shock wave experiments on porous calcite (Dover chalk, 54% crystal density) up to 19 GPa using a propellant gun. In these experiments, the shocked material after isentropic expansion impacted against an Al witness plate backed by a LiF window. The particle velocity history of the Al/LiF interface was monitored using a VISAR interferometer [15]. The behavior of calcite was studied by comparing numerical simulation profiles with experimental ones [1]. That study suggested that the shock-induced devolatilization of single-crystal calcite occurs after unloading from 18 GPa and, of course, to a greater degree upon release from higher shock pressures.

Temperature measurements along the Hugoniot are very useful for detecting and characterizing both polymorphic phase transitions [16] and molecular dissociation [17]. (Some of our results were analyzed recently by Ivanov and Deutsch [18].) In the present work, we report for planar shock compressed crystalline calcite measurements in which six 5.0 nm wide visible and near infrared radiances versus time are recorded at 1 ns intervals and inverted to yield shock temperatures in the 95–160 GPa pressure range. Also, we have performed model calculations for shock temperatures in calcite. The comparison of measurements and calculations demonstrates that temperatures are lower than if melting and/or devolatilization of calcite are not occurring. Since the temperature deficit is much greater than that expected from melting alone, it is inferred that shock-induced decomposition of calcite occurs behind the shock front. High-speed photographic recording, employing a streak camera, indicates

the occurrence of transient heterogeneous processes in shocked calcite.

2. Experiments

Experiments were performed on the two-stage light gas gun (pump tube length 6 m, diameter 89 mm; launch tube length 5.7 m, diameter 25 mm) at the Lindhurst laboratory. The 0.5 mm thick Ta flyer plates molded onto Lexan projectiles were accelerated to velocities of 5.0–6.9 km/s and impacted target assemblies (Fig. 1). These consisted of 0.5 mm thick Ta driver plates in contact with the samples. Optically flawless samples of single-crystal calcite were obtained in the form of discs, 12.7 mm in diameter and 3 mm thick, from the Karl Lambrecht Inc. The average bulk density of the samples was measured to be 2.665 ± 005 g/cm^3. The impact of a Ta flyer plate induces a shock wave in the driver plate, which then propagates through the sample. The hot luminous shock propagates across the sample in $\sim$200 ns. The optical radiation from the shock-heated sample is directed into a six-channel optical pyrometer [14]. Precautions were taken to minimize light from unwanted sources from entering the pyrometer. For example, the surface of the sample facing the driver plate was sputter-coated with a 1500 Å thick layer of silver. A silver film of this thickness is opaque to optical and near-infrared light. Silver, having a higher shock impedance than calcite, will not emit sufficient light to be detected against a bright background of the always much hotter shocked crystal calcite. This is used to block any direct radiation emitted from the shock-heated driver plate and also to suppress the 'gap flash' emission from residual gases resulting from the shock arrival at the driver–sample interface. The free surface side of the sample was covered with an annular mask that blocked emission from the edges of the sample, which are affected by the release wave. The mask also controls the light flux from the experiment to avoid saturating the optical pyrometer photodetectors.

The layout of the optical pyrometer is shown in Fig. 2. The optical radiation from the sample passes through the hole in the mask, reflects at a sacrificial turning mirror, passes through an optical window at the port of the target chamber, and finally focuses through a lens onto a bundle of optical fibers. The fiber bundle distributes light evenly to six channels through wideband filters in the wavelength range of 450–900 nm. The optical bandwidth of each channel is $\sim$5.0 nm and these are centered at wavelengths of 451.5, 555.5, 603.7, 661.5, 748.2, 904.0 nm. The light intensity is measured via a photo-detector (Model 1801, New Focus, Inc.), which consists of a photodiode and a built-in preamplifier with a 125 MHz bandwidth and 3 ns rise time. The detector signals are recorded with 500 MHz and 1 GHz sampling rate

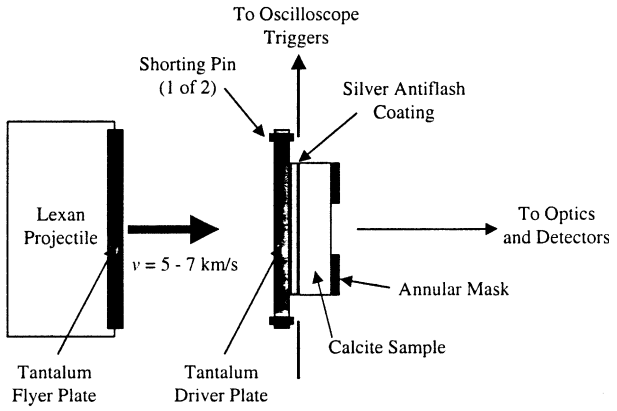

Fig. 1. Sketch of projectile and target assembly. Projectile consists of Lexan sabot and tantalum impactor. Target assembly consists of tantalum driver plate and single-crystal calcite sample with silver coating on one surface and annular mask on the other surface.

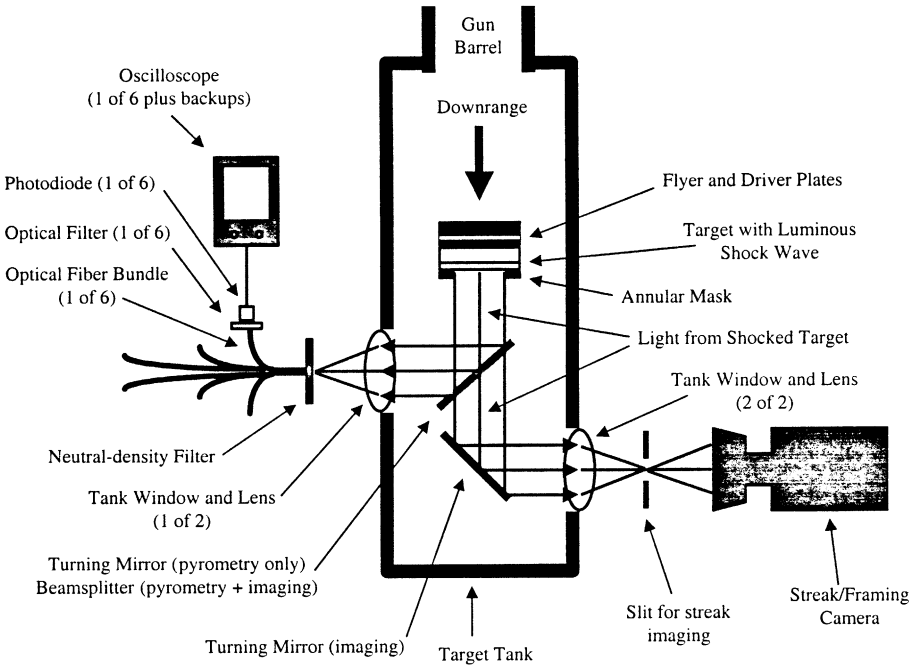

Fig. 2. Sketch of experimental setup. Light from shock material passes through transparent unshocked portion and escapes through hole in center of mask. Sacrificial turning mirror within evacuated target tank directs optical path through window into a bundle of optical fibers, which distributes the light equally through six broad band optical filters (center wavelengths 451.5, 555.5, 603.7, 661.5, 748.2, and 904.0 nm). Light intensity is detected by a photodiode, amplified, and recorded with high-speed digital oscilloscopes.

Gould (Model 4074) and Hewlett-Packard (Models 54111D and 54540) digital oscilloscopes. We calibrate the optical pyrometer prior to each shot with a NIST-certified 1000 W standard light source (Optronic Laboratory lamp, Model OL200M, driven using an Optronic, Model 83A, power supply). For calibration, the standard source is placed in the target chamber at the position later occupied by the sample so that the light from the calibration source passes through the optical system in precisely the same configuration as in the experiment. The voltage data from the oscilloscopes are converted into absolute intensities using the NIST standard lamp certification.

A typical oscilloscope record from one of the pyrometer channels is shown in Fig. 3. This signal shows a sharp peak of 10 ns width, followed by a steady (plateau) value for about 80 ns, and then a slow increase. The initial sharp peak could be associated with initial 'gap flash' arising due to discontinuities between the target and driver plate, and due to imperfection in the flash suppressant silver coating. The plateau voltage represents the light from the shock-heated sample. The slow increase beyond 120 ns is attributed to the late time increase in light or emission from the sample lateral surface that becomes scattered into the field of view of the pyrometer.

The plateau voltage level, obtained as the average value from a time period of 40–110 ns of shock propagation for each channel of pyrometer, is used for temperature determination. Temperature and emissivity are determined by fitting the spectral intensities at six wavelengths to the gray-body Planck spectrum:

$$N(\lambda) = \frac{\varepsilon C_1}{\lambda^5}(e^{c_2/\lambda T} - 1)^{-1}$$

where $N(\lambda)$ is the measured intensity at wave-

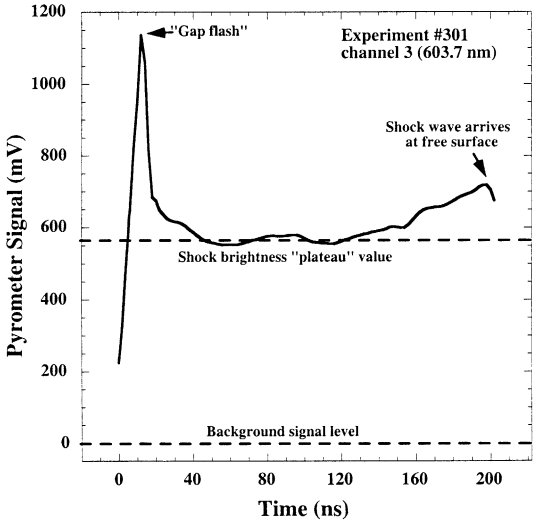

Fig. 3. Oscilloscope trace from a typical pyrometer channel (channel 3, 603.7 nm center wavelength, Expt. 301). Strong 'entrance flash' is attributable to discontinuities between driver and target plates, and to imperfections in silver flash-suppressant coating. Dashed line indicates the 'plateau' used to calculate the shock temperature. Signal growth towards end of experiment is attributable to light emission from sample lateral surfaces that become scattered into the field of view of the pyrometer.

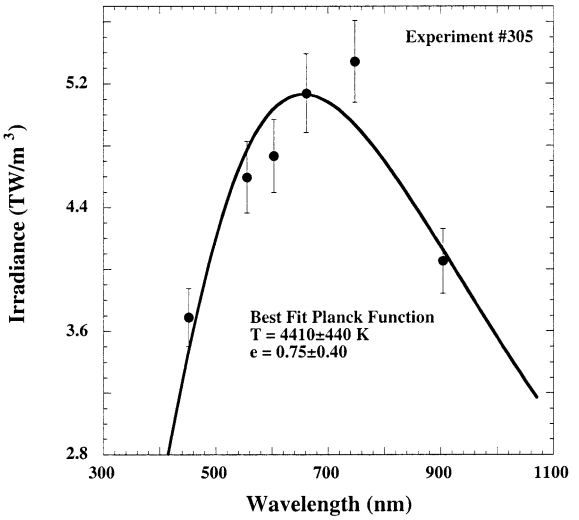

Fig. 4. Sample fit of pyrometer radiance to a Planck gray-body function for a typical experiment (#305). Error bars are estimated from uncertainty in plateau value.

length λ, ε is the emissivity assumed to be constant, T is the temperature, $C_1 = 1.191 \times 10^{-16}$ W/m^2/sr, and $C_2 = 0.01438$ mK. Fig. 4 displays typical pyrometer intensities (Expt. 305) along with our best fit Planck function.

Shock temperature results from six experiments, in the pressure range 95–160 GPa, are summarized in Table 1. Projectile velocities have been measured. Shock pressures in the sample are determined by performing impedance match calculations employing measured flying plate velocity and known Hugoniots of tantalum [19] and calcite [20,21]. The available experimental Hugoniot relation between shock velocity and particle velocity is found to be linear in the pressure range 10.5–94.4 GPa [21]. We assumed this relation to be valid for higher pressures in the present experiments.

The uncertainties in the present temperature and emissivity results arise mainly from errors in estimating plateau and background voltage val-

Table 1
Measured temperatures and emissivities of calcite

Shot No.	Sample No.	Impact velocity[a] (km/s)	Pressure[b] (GPa)	Temperature (K)	Emissivity
299	2	6.93 ± 0.01	158.3 ± 1.6	5430 ± 540	0.55 ± 0.40
298	1	6.71 ± 0.01	150.0 ± 1.5	5040 ± 1000	1.10 ± 0.40
300	3	6.37 ± 0.01	138.8 ± 1.4	5425 ± 600	0.77 ± 0.40
301	5	6.00 ± 0.01	126.3 ± 1.3	4530 ± 450	1.60 ± 0.40
305	7	5.48 ± 0.01	110.0 ± 1.1	4410 ± 440	0.75 ± 0.40
308	6	5.00 ± 0.01	95.0 ± 1.0	3250 ± 400	1.15 ± 0.40

Projectile velocities are measured.
[a] Flyer and driver plates in all experiments are tantalum [19].
[b] Pressures are obtained by shock impedance matching.

ues. For most experiments, we made three independent assessments of the plateau, and used them to quantify these errors (usually a few percent), which were used in turn to derive error estimates for the six intensity values used in Planck curve fitting. (In cases where a channel's output signal was near 1.0 V, the limit for linearity of the photodetector, we increased the estimated uncertainty to decrease that channel's statistical weight in the fit. If the signal exceeded 1.0 V, we disregarded data from the channel.) The most significant errors arise in fitting a Planck function to the data points. Because of the finite uncertainty in data points, a range of temperatures and emissivities fit the data indistinguishably well. Boslough and Ahrens [22] estimate that the uncertainty in temperature from this effect is about 5%, and that the uncertainty in emissivity is as much as 50%. The uncertainties in our emissivity results (Table 1) seem to corroborate the estimate of Boslough and Ahrens [22]. A few emissivity values are more than unity, which is physically unreasonable. The highest emissivity value of 1.6 (Expt. 301) would demand a temperature increase of 12% to bring it down to a physically reasonable value of 1.0 with the same total light output. Thus, 12% should be taken as an upper limit to the uncertainty for the temperature presented here. We conservatively show 10% uncertainty for most of the points in Table 1 and Fig. 5. A larger uncertainty is assumed for Expt. 298 which had a fewer number of channels of useful data.

Before we proceed to carry out any analysis, it is important to ensure that the temperatures inferred from the present experiments are from calcite and not from silver, as the emissivity of silver is much higher than that of calcite at ambient pressure. We believe that the temperatures we are measuring are those of calcite due to the following reasons. (1) There is a large body of experimental data in the literature on shock-induced temperature measurements, which demonstrate that initially transparent samples acquire very large emissivity during the shock propagation and that the shock front is almost opaque [23]. (2) Even if we disregard this and assume the emissivity of calcite in the shock-compressed state (as

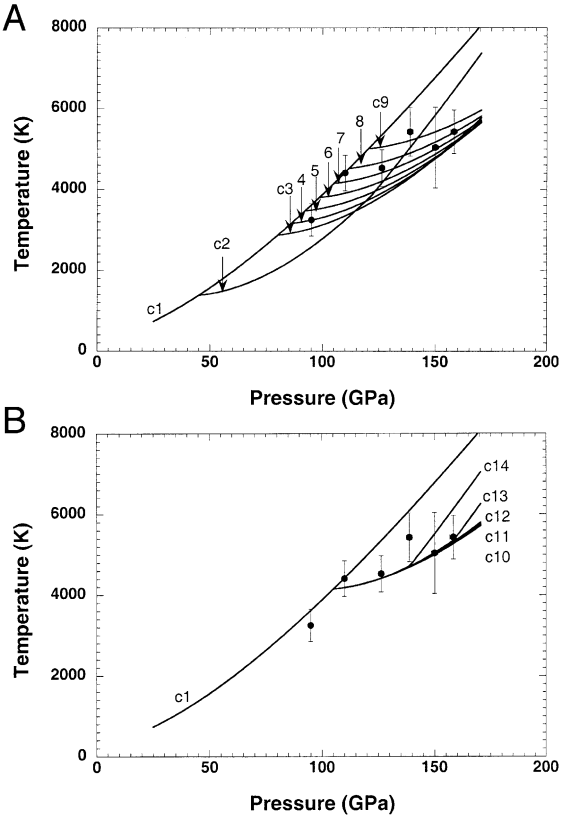

Fig. 5. Measured and calculated shock temperatures along Hugoniot. Solid circles with error bars are measurements. Error bars in pressure are about the size of solid circles. Measurements at 150 GPa have larger uncertainty in temperature as this experiment had fewer data channels. Curves represent different models. (A) c1 represents calculation without decomposition; c2 through c9 depict calculations with disproportionation; for c2, $S_I = 1.47$ and $S_V = 2.91$; for c3 through c9, S_I is incremented successively by 0.1 (keeping $S_V - S_I$ = constant) so that for c9, $S_I = 2.87$ and $S_V = 4.31$; (B) for c10 through c14, S_V values are 4.11, 3.91, 3.71, 3.51 and 3.31 respectively ($S_I = 2.67$ for all calculations). All entropies are in units of kJ(kg·K)$^{-1}$.

at ambient conditions) is low, the recorded temperature would correspond to the temperature of the interface between the sample and the silver layer deposited on the sample surface facing the driver plate. The first shock into the silver layer (due to its higher impedance) is of much higher pressure than the shock pressure in the sample. (Consequently the initial temperature in the silver layer is much higher. For example, in Expt. 308, the initial shock and temperature in the silver

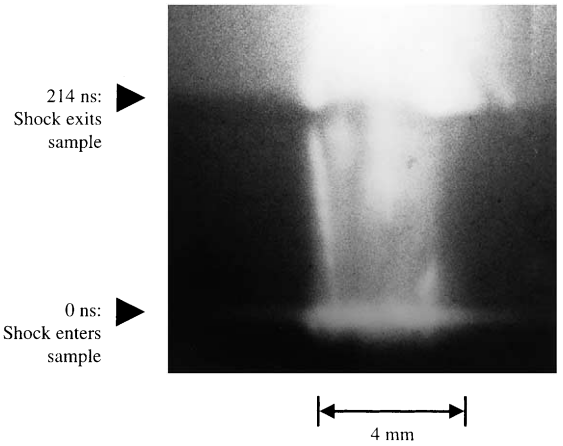

Fig. 6. Streak camera image record of Expt. 305. Time increases vertically. Bright line at bottom indicates entry of shock into sample and dark discontinuity near top marks unloading after ~214 ns. Horizontal direction denotes position along ~4 mm long linear slit. Appearance and movement of bright areas indicate occurrence of transient heterogeneous processes in sample.

layer are estimated to be 275 GPa and 8400 K, respectively.) However, within 5–10 shock reverberations in silver, which take ~0.45–0.9 ns, the silver layer shock pressure equilibrates with the shock pressures of the sample interior and the driver plate (95 GPa in case of Expt. 308). Comparison shows that the present temperatures are larger than those expected upon conduction to the silver layer from the underlying tantalum which became shock heated to a much lower temperature. During the passage of shock wave, the silver coating, being thermally conducting and only 1500 Å thick, would thermalize (through conduction) with the tantalum driver plate within 1–7 ns. So, the interface (between sample and silver) temperature would be the temperature of the Ta driver plate. Comparison shows that the present temperatures are larger than even those expected from tantalum at corresponding pressures [24]. (3) Also, the temperature signals last for ~200 ns, which is approximately equal to the transit time of shock in the calcite samples.

In one experiment (#305), we performed high-speed imaging also of the sample with a streak camera along with temperature measurements during shock loading. The streak camera record from Expt. 305 is shown in Fig. 6. The bright line at the bottom of this record marks the entry of the shock wave into the sample. As time increases, the record shows that the sample contains bright spots that appear and coalesce. The bright line in the record may indicate the movement of the bright spot. The non-uniform brightness in the record (Fig. 6) suggests occurrence of transient non-heterogeneous processes in the shocked calcite. This result is in conformity with the previous results of Kondo and Ahrens [25].

3. Model temperature calculations

For interpreting the experimental data, we have performed model temperature calculations. We assume two cases: one in which calcite does not decompose in the shocked state up to the highest shock pressure of the experiment, and another in which it disproportionates according to the chemical reaction:

$$CaCO_3 \rightarrow CaO\ (\text{solid, B1 phase}) + CO_2\ (\text{gas}) \quad (1)$$

It is clear that the disproportionation products of Eq. 1 are not established. If disproportionation occurs, it is expected that other species could be present such as CaO (B2 phase, discovered by Jeanloz and Ahrens [26]), Ca (metal), O_2 and C (diamond).

The two cases are briefly described below. The possibility of melting along the Hugoniot is also assessed.

3.1. Temperature calculation without decomposition of calcite (Model 1)

Temperature increase upon shock compression of a material to a specific volume V is calculated using the relation:

$$\int_{T_S}^{T_H} C_V dT = E_H - E_S - \Delta E_{tr} \quad (2)$$

where T_H and T_S are temperatures along Hugoniot and isentrope at the same compression and E_{tr} is phase transition energy. Isentropic temper-

ature T_S, Hugoniot energy E_H, and isentropic energy E_S are given by the following relations:

$$\gamma = \gamma_r\left(\frac{V}{V_r}\right)^q \tag{3}$$

$$T_S = T_0 \exp\left[\int_V^{V_0} (\gamma(V)/V)\mathrm{d}V\right] \tag{4}$$

$$E_H = \frac{1}{2}P_H(V_0 - V) \tag{5}$$

$$E_S = -\int_{V_r}^{V} P_S \mathrm{d}V \tag{6}$$

$$P_S = \frac{3K_0}{2}\left[\left(\frac{V_r}{V}\right)^{7/3} - \left(\frac{V_r}{V}\right)^{5/3}\right]$$
$$\left[1 + 3\left(\frac{K'_0}{4} - 1\right)\left\{\left(\frac{V_r}{V}\right)^{2/3} - 1\right\}\right] \tag{7}$$

where P_H and P_S are pressures along Hugoniot and isentrope at the same specific volume V; the specific volumes V_0 and V_r correspond to initial low-pressure phase and the shock-induced, high-pressure phase at ambient pressure; T_0 is the initial temperature; K_0 and K'_0 are the isentropic bulk modulus and its pressure derivative; γ_r is the Gruneisen ratio at specific volume V_r; and the exponent q is assumed to be equal to 1. The analytic form assumed for the isentrope is the Birch–Murnaghan equation. The entropy increase along the Hugoniot has been determined using the relation:

$$\Delta S_H = \Delta S_{tr} + \int_{T_S}^{T_H} \frac{C_V}{T}\mathrm{d}T \tag{8}$$

where ΔS_{tr} is the entropy change of phase transition between the initial phase and the phase into which the sample has been shocked. Thus ΔS_{tr} is zero if there is no phase transition, otherwise it is the entropy of the high-pressure phase relative to that of the low-pressure phase at room temperature and pressure.

3.2. Temperature calculation with disproportionation of calcite (Model 2)

For disproportionation of calcite, the entropy criterion is employed. The decomposition begins at pressure for which shock entropy equals S_I, entropy of incipient decomposition at normal pressure. The decomposition completes at pressure for which shock entropy equals S_V, the entropy of complete decomposition at normal pressure. The theoretical values of S_I and S_V are estimated from thermodynamic data on Gibbs free energies and entropies of reactants and products of the chemical reaction (Eq. 1). At normal pressure the decomposition of calcite occurs at temperature T_I at which Gibbs free energies of the reactants and the products are equal. S_I is given by entropy of calcite at T_I. The excess entropy required for complete reaction is:

$$S_V = S_I + \Delta S \tag{9}$$

with ΔS as the entropy difference between products and reactants at T_I. Using the compilation of thermodynamic data by Robie et al. [27], we have estimated the values of S_I and S_V for calcite to be 1.47 kJ(kg·K)$^{-1}$ and 2.91 kJ(kg·K)$^{-1}$, respectively. We may point out that the equilibrium of the reaction represented by Eq. 1 is strongly influenced by the ambient pressure of CO_2; the decrease in pressure of CO_2 leads to lower values of S_I and S_V (Tyburczy and Ahrens [28]). Our present theoretical estimates assume the pressure of CO_2 for the reaction in Eq. 1 to be 1 bar, which is too high for Earth and Mars and too low for Venus.

Upon shock compressions down to specific volume V_I, for which $\Delta S_H \leq S_I$, the material does not decompose. Temperature and entropy along the Hugoniot are calculated using Eqs. 2–8, as in Model 1. Decomposition of calcite is assumed to set in as the shock entropy exceeds S_I upon higher compressions (to specific volumes lower than V_I). The fraction α of decomposed calcite is determined from the entropy of shocked solid calcite using the relation:

$$\alpha = \frac{\Delta S_H - S_I}{S_V - S_I}$$

In the shocked state, material consists of α moles of each of solid CaO and gaseous CO_2 and $(1-\alpha)$ moles of the high-pressure phase of calcite. The temperature for this mixture is given by:

$$T_H = T_S + \frac{E_{HI} - E_{SI} - E_{tr}}{C_{VI}} + \frac{E_H - E_S - E_{HI} + E_{SI} - \alpha E_{sub}}{C_{V\alpha}} \quad (10)$$

E_{HI} and E_{SI} are the Hugoniot and isentropic energies corresponding to specific volume V_I; $C_{V\alpha}$ is the mass weighted heat capacity of the mixture of the solid calcite and the reaction products, and it is given by:

$$C_{V\alpha} = (1-\alpha)C_{V1} + \alpha C_{V2}$$

where C_{V1} is the heat capacity of the high-pressure phase of calcite and C_{V2} that of the mixture of reaction products. E_{sub} is the energy required for decomposing 1 mole of $CaCO_3$ (high-pressure phase), which is equal to the energy required to generate entropy increment for the disproportionation reaction (Eq. 1). It is approximated in terms of S_I, S_V and T_I (temperature of incipient disproportionation) as:

$$E_{sub} \cong T_1(S_V - S_1)$$

Eq. 10 is applicable at high pressure even when calcite (high-pressure phase) is completely transformed to CaO and CO_2, i.e., α becomes 1.

Previous shock wave measurements reported that calcite undergoes three phase transitions: calcite I to II transition between 0.6 and 1.2 GPa, calcite II to III transition around 2.4 GPa, and III to IV transition around 10 GPa [20,29]. We have used the isentrope of phase IV as the reference state. The material parameters assumed for calcite in the present calculation are listed in Table 2. Since no thermal expansivity data are available on $CaCO_3$ and CaO, which could be used to determine C_V from the measurements of Cp (specific heat at constant pressure), the Dulong–Petit values of $15R$ and $6R$ per mole of molecules have been used. For gaseous CO_2 we have estimated it from the data of specific heat at constant pressure [30]. The estimated value of $6.7R$/mole for CO_2 gas is smaller than the solid state value of $9R$/mole.

Table 2
Material properties for single-crystal calcite

Property	Value	Ref.
ρ_0	2.67 g/cm^3	a
ρ_r	3.00 g/cm^3	b
C_0	3.80 km/s	c
s	1.42	c
Γ_0	1.84	d
K_0	75.0 GPa	b
K'_0	4.1	b
C_v	1.25 kJ(kg·K)$^{-1}$	b
E_{tr}	0.20 MJ/kg	b
ΔS_{tr}	0.067 kJ(kg·K)$^{-1}$	e

a, measured value; b, [28]; c, the Hugoniot plotted in the form of shock velocity versus particle velocity in the 10.5–94.4 GPa pressure range is experimentally found to be linear; C_0 is the intercept on shock velocity axis and s is the slope of the line [21]; these C_0 and s values are assumed to be valid at higher pressures in the present experiments; d, $\Gamma_0 = 2s-1$ [33]; e, [14].

4. Results and discussions

Experimental results along with model calculations are plotted in Fig. 5. The comparison of measurements with calculations using Model 1 (curve c1 in Fig. 5A) indicates that the measured temperatures are some 400–1350 K lower than if shock-induced melting and/or decomposition is not occurring.

Static high pressure, high temperature experiments up to 3.5 GPa on calcite show that below 4 MPa it decomposes into solid CaO and gaseous CO_2 without melting, and undergoes congruent melting to a molecular liquid at pressure above 0.1 GPa, but forms a mixture of molecular liquid, solid CaO and gaseous CO_2 in the intermediate pressure range [31]. We have assessed the influence of melting on our shock temperature mea-

surements. We assume the entropy of fusion to be approximately equal to gas constant R per mole of atoms, the same as those of simple elements [32]. The value 0.41 kJ(kg·K)$^{-1}$ for calcite is about 28% of the value of entropy of vaporization. The temperature deficit estimated for calcite is $\sim$450 K. Melting of calcite behind the shock front may be occurring; however, even if it is occurring the resulting temperature decrease due to congruent melting is too small to account for the observed temperature deficit. This implies that devolatilization of calcite behind the shock front is taking place.

In Fig. 5A, curves c2 through c9 show the calculations using Model 2 in which calcite begins to decompose at S_I and completes at S_V. Curve c2 corresponds to the theoretical values of entropies $S_I = 1.47$ kJ(kg·K)$^{-1}$ and $S_V = 2.91$ kJ(kg·K)$^{-1}$. Curves c3 through c9 depict calculations in which larger than theoretical values of S_I and S_V are used. For calculation c3, S_I is 2.27 kJ(kg·K)$^{-1}$ and S_V is 3.71 kJ(kg·K)$^{-1}$; for other calculation (c4–c9), the values of S_I and S_V are successively incremented in steps of 0.1 kJ(kg·K)$^{-1}$ (keeping $S_V - S_I$ constant) until for calculation c9 these are 2.87 and 4.31 kJ(kg·K)$^{-1}$, respectively.

Fig. 5 shows that curve c2 lies below the experimental data, suggesting that the decomposition does not begin at the pressure at which shock entropy equals the theoretical estimates of S_I but it sets in when the system is overdriven to higher pressures. Considering the uncertainties in the experimental data, the comparison through visual inspection of all the calculations with measurements shows that calculations c7 and c8 closely match the present measurements. This suggests that the chemical disproportionation of calcite behind the shock front begins around 110 ± 10 GPa.

Calculations are also performed by fixing the values of S_I at 2.67 and varying S_V. For calculations c10 through c14, S_V values are 4.11, 3.91, 3.71, 3.51, and 3.31 kJ(kg·K)$^{-1}$, respectively. Fig. 5B shows that calculations c10, c11 and c12 do not differ from each other in the pressure range of the experiment (these, however, differ at higher pressures). Calculation c14 deviates from the experimental data suggesting that the lower bound of S_V is 3.31 kJ(kg·K)$^{-1}$.

The pressure of disproportionation 110 ± 10 GPa obtained above is higher than the 18 GPa pressure at which calcite begins to decompose on unloading. The 18 GPa value is based on the comparison of VISAR measurements of particle velocity profile induced upon isentropic expansion with one-dimensional numerical simulation [1]. The higher pressure for the onset of chemical decomposition at the shock front could be due to kinetic effects, as the time available for the reaction to occur within a few nanosecond duration of temperature measurements at the shock front is much smaller than in a few microsecond duration of VISAR experiments involving isentropic release subsequent to loading.

In the above analysis, the shock compressed state is assumed to be in thermal equilibrium during a few nanosecond period over which the temperature measurements are carried out. This is reasonable, as the characteristic times of phonon–phonon and electron–phonon interactions (which bring about equilibrium) are less than a picosecond. The shock-induced disproportionation of calcite may be accompanied by a large volume change, which is expected to cause anomaly in the Hugoniot also. So far, the Hugoniot of calcite has been measured up to 94.4 GPa [21]. It will be very interesting to perform Hugoniot measurement at higher pressures and look for the signature of the calcite disproportionation.

5. Conclusions

Shock temperatures in single-crystal calcite have been measured at 95–160 GPa in a two-stage light gas gun using optical pyrometry. Model calculations have been performed for shock temperatures in this material. Comparison of the measured and calculated temperatures suggests that the onset of decomposition in calcite to CaO and CO_2 occurs at $\sim 110 \pm 10$ GPa. This decomposition pressure is higher than 18 GPa from which pressure calcite begins decomposing upon unloading.

Acknowledgements

Research supported by NASA. We thank Kathleen Holland, Mike Long, Papo Gelle, and Alberto De Vora for technical help and assistance with this work. S.C.G. wishes to thank S.K. Sikka for his encouragement and support. Helpful suggestions of Toshimori Sekine and D.L. Heinz are thankfully acknowledged. Contribution No. 8677 Division of Geological and Planetary Sciences (Caltech).*[RV]*

References

[1] S.C. Gupta, T.J. Ahrens, W. Yang, Shock-induced vaporization of anhydrite $CaSO_4$ and calcite $CaCO_3$, in: M.D. Furnish, L.C. Chhabildas, R.S. Hixson (Eds.), Shock Compression of Condensed Matter – 1999, AIP, Woodbury, NY, 2000, pp. 1259–1262.

[2] E.R.D. Scott, A.N. Krot, A. Yamaguchi, Carbonates in fractures on Martian meteorite Allan Hills 84001: petrologic evidence for impact origin, Meteor. Planet. Sci. 33 (1998) 709–719.

[3] J.S. Kargel, R.L. Kirk, B. Fegley Jr., A.H. Treiman, Carbonate sulfate volcanism on Venus, Icarus 112 (1994) 219–252.

[4] L.E. Alvarez, W. Alvarez, F. Asaro, H.V. Michel, Extraterrestrial cause for the Cretaceous-Tertiary extinction, Science 208 (1980) 1095–1108.

[5] K.O. Pope, K.H. Baines, A.C. Ocampo, B.A. Ivanov, Energy, volatile production, and climatic effects of the Chicxulub Cretaceous/Tertiary impact, J. Geophys. Res. 102 (E9) (1997) 21645–21664.

[6] R. Brett, The Cretaceous-Tertiary extinction: a lethal mechanism involving anhydrite target rocks, Geochim. Cosmochim. Acta 56 (1992) 3603–3606.

[7] K.O. Pope, K.H. Baines, A.C. Ocampo, B.A. Ivanov, Impact winter and the Cretaceous – Tertiary Extinctions – Results of a Chicxulub Asteroid Impact Model, Earth Planet. Sci. Lett. 128 (1994) 719–725.

[8] J.D. O'Keefe, T.J. Ahrens, Impact production of CO_2 by Cretaceous/Tertiary extinction bolide and the resultant heating of the Earth, Nature 338 (1989) 247–249.

[9] S.W. Kieffer, C.H. Simonds, The role of volatiles and lithology in the impact cratering process, Rev. Geophys. Space Phys. 18 (1980) 143–181.

[10] J. Vizgirda, T.J. Ahrens, Shock compression of aragonite and implication for equation of state of carbonates, J. Geophys. Res. 87 (1982) 4747–4758.

[11] M.B. Boslough, T.J. Ahrens, J. Vizgirda, R.H. Becker, S. Epstein, Shock-induced devolatilization of calcite, Earth Planet. Sci. Lett. 61 (1982) 166–170.

[12] M.A. Lange, T.J. Ahrens, Shock-induced CO_2 loss from $CaCO_3$: implications for early planetary atmospheres, Earth Planet. Sci. Lett. 77 (1986) 409–418.

[13] D.E. Grady, Processes occurring on shock wave compression of rocks and minerals, in: M.H. Manghnani, S. Akimoto (Eds.), High Pressure Research: Applications in Geophysics, Academic Press, New York, 1977, pp. 389–438.

[14] W. Yang, Impact volatilization of calcite and anhydrite and the effects on global climate from the K/T impact crater at Chicxulub, Ph.D. thesis, California Institute of Technology, Pasadena, CA, 1996.

[15] L.M. Barker, R.E. Hollenbach, Laser interferometer for measuring high velocities of any reflecting surface, J. Appl. Phys. 43 (1972) 4669–4675.

[16] K.G. Holland, T.J. Ahrens, Melting of $(Mg,Fe)_2SiO_4$ and the core-mantle boundary of the Earth, Science 275 (1997) 1623–1625.

[17] H.B. Radousky, W.J. Nellis, M. Ross, D.C. Hamilton, A.C. Mitchell, Molecular dissociation and shock-induced cooling in fluid nitrogen at high densities and temperatures, Phys. Rev. Lett. 57 (1986) 2419–2422.

[18] B.A. Ivanov, A. Deutsch, The phase diagram of $CaCO_3$ in relation to shock compression and decomposition, Phys. Earth Planet. Int. 129 (2002) 131–143.

[19] A.C. Mitchell, W.J. Nellis, Shock compression of aluminum, copper, and tantalum, J. Appl. Phys. 52 (1981) 3363–3374.

[20] T.J. Ahrens, J.V.G. Gregson, Shock compression of crustal rocks: data for quartz, calcite, and plagioclase rocks, J. Geophys. Res. 69 (1964) 4839–4874.

[21] N.G. Kalashnikov, M.N. Pavlovskiy, G.V. Simakov, R.F. Trunin, Dynamic compressibility of calcite-group minerals, Izv. Earth Phys. 2 (1973) 23–29.

[22] M.B. Boslough, T.J. Ahrens, A sensitive time-resolved radiation pyrometer for shock-temperature measurements above 1500 K, Rev. Sci. Instrum. 60 (1989) 3711–3716.

[23] S.B. Kormer, Optical study of the characteristics of shock-compressed dielectrics, Sov. Phys. Uspekhi 11 (1968) 229–254.

[24] R.G. McQueen, S.P. Marsh, J.W. Taylor, J.N. Fritz, W.J. Carter, The equation of state of solids from shock wave studies, in: R. Kinslow (Ed.), High-Velocity Impact Phenomena, Academic Press, New York, 1970, pp. 293–417.

[25] K.-I. Kondo, T.J. Ahrens, Heterogeneous shock-induced thermal radiation in minerals, Phys. Chem. Miner. 9 (1983) 173–181.

[26] R. Jeanloz, T.J. Ahrens, H.K. Mao, P.M. Bell, B1/B2 transition in CaO from shock-wave and diamond cell experiments, Science 206 (1979) 829–830.

[27] R.A. Robie, B.S. Hemingway, J.R. Fisher, Thermodynamic properties of minerals and related substances at 298.15 K and 1 bar (10^5 pascals) pressure and at higher temperatures, US Geol. Surv. Bull. 1452 (1979) 456.

[28] J.A. Tyburczy, T.J. Ahrens, Dynamic compression and volatile release of carbonates, J. Geophys. Res. 91 (1986) 4730–4744.

[29] D.E. Grady, R.E. Hollenbach, K.W. Schuler, Compression wave studies on calcite rock, J. Geophys. Res. 83 (1978) 2839–2849.
[30] G.V. Belov, B.G. Trusov, ASTD Computer Aided Reference Book in Thermodynamics and Thermophysical Properties of Species, Version 2, C1983–1999, Moscow, 1999.
[31] A.J. Irving, P.J. Wyllie, Subsolidus and melting relationships for calcite, magnesite, and the joint $CaCO_3$-$MgCO_3$ to 36 kbar, Geochim. Cosmochim. Acta 39 (1975) 35–53.
[32] S.M. Stishov, Melting at high pressures, Sov. Phys. Uspekhi 11 (1969) 816–830.
[33] A.L. Ruoff, Linear shock-velocity-particle-velocity relationship, J. Appl. Phys. 38 (1967) 4976–4980.